ChemComm

Cathodic electrogenerated chemiluminescence of tris(2,2′-bipyridine)ruthenium(II) and peroxydisulfate at pure $Ti_3C_2T_x$ MXene electrodes

Journal:	*ChemComm*
Manuscript ID	CC-COM-04-2020-002993.R1
Article Type:	Communication

COMMUNICATION

Cathodic electrogenerated chemiluminescence of tris(2,2'-bipyridine)ruthenium(II) and peroxydisulfate at pure $Ti_3C_2T_x$ MXene electrodes

Received 00th January 20xx,
Accepted 00th January 20xx

DOI: 10.1039/x0xx00000x

Jizhen Zhang[a,†], Emily Kerr [a,†,*], Ken Aldren S. Usman[a], Egan H. Doeven [b], Paul S. Francis [c], Luke C. Henderson [a,*] and Joselito M. Razal [a,*]

We demonstrate the first use of pure films of two-dimensional (2D) transition metal carbides and nitrides ($Ti_3C_2T_x$ MXene) as an electrode material for electrogenerated chemiluminescence (ECL). The $Ti_3C_2T_x$ MXene electrodes exhibited excellent electrochemical stability in the cathodic scan range and produced bright reductive-oxidation ECL using peroxydisulfate as a co-reactant with the tris(2,2'-bipyridine)ruthenium(II) ($[Ru(bpy)_3]^{2+}$) luminophore.

Electrogenerated chemiluminescence (ECL) is a sensitive analytical technique where highly exergonic electron transfer reactions occur between electrochemically generated radical species at the surface of an electrode resulting in the emission of light.[1] Various ECL generation mechanisms harness the diverse properties of different electrode materials, luminophores, co-reactants, solvents and electrolytes.[1, 2] Early ECL experiments exploited the annihilation of oxidised and reduced species to form excited state products.[3] Although this strategy produced bright luminescence, it is limited to organic solvents with wide potential windows to access both the oxidation and reduction of the luminophore. This drawback was overcome by the addition of a co-reactant – a species that forms a strongly oxidising/reducing species upon reduction/oxidation – to the system.[4]

The vast majority of research has focused on the investigation of the tris(2,2'-bipyridine)ruthenium(II) ($[Ru(bpy)_3]^{2+}$) luminophore and oxidative-reduction co-reactant tri-*n*-propylamine (TPA).[5] Oxidative-reduction co-reactants have typically been favoured over reductive-oxidation co-reactants because a single oxidative potential (~1.1 V *vs* normal hydrogen electrode, NHE) can be applied to initiate light emission below the potential of water oxidation (1.23 V *vs* NHE) minimising deleterious side reactions and enhancing the sensitivity of the analysis.[5]

Different electrode materials offer distinct advantages for ECL based sensing applications.[2] For example, nanostructured carbon electrode materials, such as carbon nanotubes and graphene, often exhibit superior sensitivity in analytical ECL sensing applications when compared to traditional materials.[6] Boron-doped-diamond (BDD) can exhibit a larger accessible potential window in water (-1.25 to +2.3 V *vs* NHE),[7] when compared to conventional electrode materials such as glassy carbon (-0.3 to +1.8 V *vs* NHE),[7] due to a higher hydrogen evolution potential, thus providing opportunities to explore different luminophore/co-reactant combinations. Recently Einaga *et al*.[8] used BDD films to demonstrate the reductive-oxidation co-reactant ECL of the $[Ru(bpy)_3]^{2+}$-peroxydisulfate system in aqueous solution.

Two-dimensional (2D) transition metal carbides and nitrides, known as MXenes, are a new class of materials that show promising properties for electrochemical sensing.[9] MXenes have predominantly been incorporated in composite films with Nafion® or used to modify the properties of existing electrode materials (e.g. carbon or gold).[9, 10] The high electrical conductivity of the MXenes reduces the charge transfer resistance of the composite or electrode, thereby reducing noise and dramatically enhancing sensitivity.[10]

Recently, researchers have combined the superior conductive properties of MXenes with ECL detection strategies.[9, 11-13] For example, Liu and Xu *et al*.[11] combined $Ti_3C_2T_x$ MXene, $[Ru(bpy)_3]^{2+}$ and Nafion in a composite film for the detection of single-nucleotide mismatch in human urine using ECL. Although electrochemical sensing methods using $Ti_3C_2T_x$ MXene modified electrodes enhance the sensing properties of the conventional electrode material, they do not fully exploit the unique properties of pure $Ti_3C_2T_x$ MXenes such as their high surface area, superior conductivity (~10000 S cm^{-1})[14] and cathodic stability.

Herein, we establish the first use of pure $Ti_3C_2T_x$ MXene films as electrodes for ECL generation and explore their potential use for $[Ru(bpy)_3]^{2+}$-peroxydisulfate cathodic ECL.

[a] *Institute for Frontier Materials, Deakin University, Geelong, Victoria 3220, Australia.*
[b] *Centre for Regional and Rural Futures, Deakin University, Geelong, Victoria 3220, Australia.*
[c] *School of Life and Environmental Sciences, Deakin University, Geelong, Victoria 3220, Australia.*
† Denotes equal contribution.
* To whom correspondence should be addressed, emily.kerr@deakin.edu.au, luke.henderson@deakin.edu.au, joselito.razal@deakin.edu.au
Electronic Supplementary Information (ESI) available including experimental information and supplementary figures. See DOI: 10.1039/x0xx00000x

We synthesised $Ti_3C_2T_x$ MXene by etching Ti_3AlC_2 MAX phase (1 g) with LiF (1.6 g) and HCl solution (9 M, 20 mL), as described in detail in our previous works.[15-17] The complete etching of the aluminium layer from the MAX phase is shown by the disappearance of (014) peak on XRD spectrum of $Ti_3C_2T_x$ MXene (Figure 1a). Meanwhile, the (002) peak shifted from ~9.8° of 2 theta to ~7.0°, corresponding to an increase in layer spacing between $Ti_3C_2T_x$ MXene flakes due to water and lithium intercalation.[18-20] The advantage of the *in situ* HF method is that $Ti_3C_2T_x$ MXene flakes self-exfoliate into single-layer flakes during the repeated shaking and centrifugation steps. The obtained single-layer $Ti_3C_2T_x$ MXene flakes showed an average layer thickness of 1.8 nm and mean lateral size of ~0.9 µm (Figure 1b-d).[21] Without using sonication during the exfoliation of $Ti_3C_2T_x$ MXene, the high resolution XPS spectrum shows a negligible signal from TiO_2 on the $Ti_3C_2T_x$ MXene electrode (Figure S1), suggesting our fabricated $Ti_3C_2T_x$ MXene film electrodes are composed of pristine $Ti_3C_2T_x$ MXene flakes with minimal degradation of the electrode surface.

To prepare $Ti_3C_2T_x$ MXene electrodes, we first removed the carbon working electrodes from commercial electrodes using a sharp blade. The $Ti_3C_2T_x$ MXene dispersion was blade-coated on the same position using removable tape as a mask (Figure 1e). SEM shows that the fabricated $Ti_3C_2T_x$ MXene electrodes have a thickness of ~450 nm with well-aligned $Ti_3C_2T_x$ MXene flakes (Figure 1f). The $Ti_3C_2T_x$ MXene electrodes exhibited excellent conductivity of 8100 S cm^{-1} compared to traditional electrode materials such as glassy carbon (< 200 S cm^{-1}).[22] Our electrodes, similar to commercially available SPEs, are designed to be implemented as single-use, disposable SPEs. The blade-coating fabrication technique is simple, low-tech and cost-effective, making $Ti_3C_2T_x$ MXene film electrodes ideal candidates for single-use, point-of-care sensing applications where disposable electrodes are preferable.

We evaluated the electrochemical properties of the $Ti_3C_2T_x$ MXene electrode films using $[Ru(NH_3)_6]^{3+}$, a thoroughly studied, outer sphere, single electron transfer reaction.[23] $[Ru(NH_3)_6]^{3+}$ exhibited a reduction potential at -232 mV *vs* Ag/AgCl (Figure 2a, S2). The peak-to-peak separation (ΔE_p) of the forward and reverse sweep was large (330 mV) compared to the ideal value (ΔE_p = 59 mV), indicating that electron transfer of $[Ru(NH_3)_6]^{3+}$ is not electrochemically reversible at the $Ti_3C_2T_x$ MXene electrode surface. A large ΔE_p is common for SPEs; Kadara *et al.* previously evaluated several varieties of commercially available SPEs and reported ΔE_p values ranging from 98 to 535 mV.[24] A large ΔE_p may arise from numerous factors such as oxidation of the electrode surface by environmental oxygen, the thickness of $Ti_3C_2T_x$ MXene film electrodes, wettability of the electrode surface and the electrode drying/curing processes.[24, 25] Our electrodes exhibited reversible electrochemistry in the cathodic scan range and there was no notable change in the resulting current over multiple scans (Figure S3). However, scanning anodically caused irreversible oxidation of the $Ti_3C_2T_x$ MXene electrode surface (Figure S4) as observed by Lorencová *et al.*[10] Degassing electrolyte solutions prior to analysis reduced this passivation (Figure S4).

Initially, we investigated the most commonly used aqueous co-reactant ECL system, TPA with $[Ru(bpy)_3]^{2+}$. However, we observed no ECL from the $Ti_3C_2T_x$ MXene film working electrode presumably due to oxidation of the MXene film in the anodic scan range.[26] When we scanned the electrodes at cathodic potentials in solutions of TPA with $[Ru(bpy)_3]^{2+}$ we observed an intense ECL signal using the PMT (Figure S5). Dark-field photography confirmed this ECL emanated from $[Ru(bpy)_3]^{2+}$ reacting with TPA co-reactant, oxidised at the carbon black

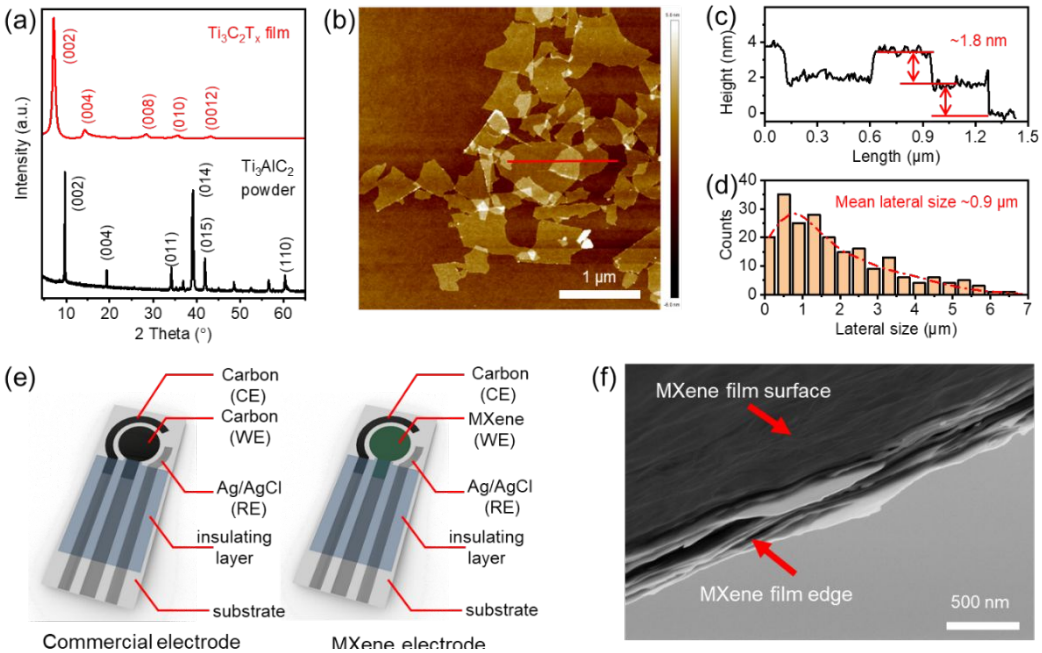

Figure 1. (a) XRD patterns of Ti_3AlC_2 MAX phase powder and drop-casted $Ti_3C_2T_x$ MXene film from as synthesised MXene suspension. (b) AFM image of $Ti_3C_2T_x$ MXene flakes on silicon wafer. (c) The profile of layer thickness along the red line in (b). (d) The lateral size distribution of $Ti_3C_2T_x$ MXene flakes measured from AFM images. (e) The commercial screen-printed electrodes (left) and $Ti_3C_2T_x$ MXene electrode (right) fabricated by changing the working electrode (WE) from carbon to $Ti_3C_2T_x$ MXene while keeping the same counter electrode (CE, carbon) and reference electrode (RE, Ag/AgCl). (f) The SEM image of the cross-section of blade coated $Ti_3C_2T_x$ MXene electrode.

counter electrode (Figure S5).[26-28] As the $Ti_3C_2T_x$ MXene electrodes were electrochemically stable in the cathodic scan range, we evaluated their potential for analytical ECL applications using a model reductive-oxidation co-reactant, peroxydisulfate. Peroxydisulfate is a versatile co-reactant that has been combined with numerous luminophores to produce sensitive analytical ECL detection systems.[8, 29-37] We combined peroxydisulfate with $[Ru(bpy)_3]^{2+}$ (outlined in equation 1 to 9) to investigate the potential of $Ti_3C_2T_x$ MXene film electrodes as a novel material for future analytical ECL sensing applications.[8, 38]

$S_2O_8^{2-} + e^- \rightarrow S_2O_8^{\bullet 3-}$ (1)

$[Ru(bpy)_3]^{2+} + e^- \rightarrow [Ru(bpy)_3]^{+}$ (2)

$[Ru(bpy)_3]^{+} + S_2O_8^{2-} \rightarrow [Ru(bpy)_3]^{2+} + S_2O_8^{\bullet 3-}$ (3)

$S_2O_8^{\bullet 3-} \rightarrow SO_4^{2-} + SO_4^{\bullet -}$ (4)

$[Ru(bpy)_3]^{+} + SO_4^{\bullet -} \rightarrow [Ru(bpy)_3]^{2+*} + SO_4^{2-}$ (5)

$[Ru(bpy)_3]^{2+} + SO_4^{\bullet -} \rightarrow [Ru(bpy)_3]^{3+} + SO_4^{2-}$ (6)

$[Ru(bpy)_3]^{3+} + [Ru(bpy)_3]^{+} \rightarrow [Ru(bpy)_3]^{2+*} + [Ru(bpy)_3]^{2+}$ (7)

$[Ru(bpy)_3]^{2+*} \rightarrow [Ru(bpy)_3]^{2+} + h\nu$ (8)

$[Ru(bpy)_3]^{2+*} + S_2O_8^{2-} \rightarrow [Ru(bpy)_3]^{3+} + SO_4^{2-} + SO_4^{\bullet -}$ (9)

The $Ti_3C_2T_x$ MXene electrodes displayed bright orange ECL from $[Ru(bpy)_3]^{2+}$ at potentials past the reduction of both peroxydisulfate and $[Ru(bpy)_3]^{2+}$ (Figure S6e and S6f).[38] The ECL from $[Ru(bpy)_3]^{2+}$ increased when the applied potential was scanned from -1.6 V to -2.5 V (Figure 2b). The ECL intensity was higher at low pH, especially at increasingly negative potentials (-2.25 V); this is consistent with previous observations and results from decreased quenching of sulfate radical anions by hydroxyl ions in accordance with equation 10.[39] At potentials more negative than -2.25 V, the electrode films became unstable, resulting in a decrease in both the ECL and current (Figure S6). The $[Ru(bpy)_3]^{2+}$-peroxydisulfate ECL from the novel $Ti_3C_2T_x$ MXene electrodes, was 7-fold higher than the ECL observed at a carbon SPE (relative integrated area of cyclic voltammogram (CV) from Figure 2b, pH 7.4). Furthermore, the signal at the $Ti_3C_2T_x$ MXene electrodes exhibited superior stability over successive scans (Figure S6D and Table S1) and the signal to blank ratio for the $Ti_3C_2T_x$ MXene electrodes was double that observed from the carbon SPEs.

$SO_4^{\bullet -} + OH^- \rightarrow SO_4^{2-} + OH^{\bullet}$ (10)

Previous literature indicates that ECL from $[Ru(bpy)_3]^{2+}$ is oxidatively quenched at high concentrations of peroxydisulfate.[38, 40] We therefore investigated the dependence of ECL intensity on peroxydisulfate concentration (Figure 3a). We observed a maximum ECL intensity at peroxydisulfate concentrations of 25 mM; above this concentration, the ECL of $[Ru(bpy)_3]^{2+}$ was quenched in accordance with equation 9. A small ECL signal was observed from PBS blank solutions, most likely resulting from the emission of excited oxygen species ($^1O_2$, $^1(O_2)_2$ and $^3(O_2)_2$), formed as a result of reduction of peroxydisulfate (Figure S6b).[8, 41, 42]

The optimised $Ti_3C_2T_x$ MXene ECL conditions exhibited a wide linear range from 100 nM to 10 µM $[Ru(bpy)_3]^{2+}$ ($R^2 = 0.9914$) and an excellent detection limit of 100 nM (signal/blank = 3). Bard *et al.*[42] detected ECL from $[Ru(bpy)_3]^{2+}$ in 1:1 water:acetonitrile solutions at 10 nM at carbon and platinum disk electrodes. When degassed, ECL from 100 fM $[Ru(bpy)_3]^{2+}$ could be observed.[42] Previous work by Einaga *et al.*[8] using BDD electrodes in aqueous solutions showed ECL at $[Ru(bpy)_3]^{2+}$-peroxydisulfate ratios as low as 1/1000 (10 µM/10 mM). In this work, we detected ECL at a $[Ru(bpy)_3]^{2+}$-peroxydisulfate ratio of 1/250000 (100 nM/25 mM). This dramatically improves upon the previously documented accessible ranges of $[Ru(bpy)_3]^{2+}$ detection with peroxydisulfate

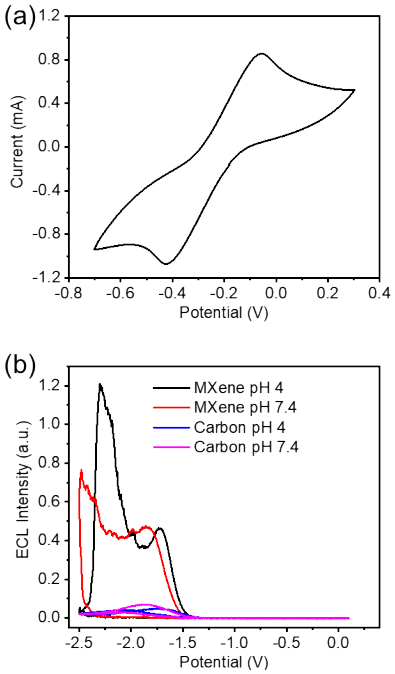

Figure 2. (a) CV of 25 mM $[Ru(NH_3)_6]^{3+}$ in PBS, pH 7.4, 0.1 V s^{-1}. (b) ECL intensity of 5 µM $[Ru(bpy)_3]^{2+}$ and 25 mM $S_2O_8^{2-}$ in PBS using 5 mm diameter $Ti_3C_2T_x$ MXene film and carbon SPEs, scan rate 0.25 V s^{-1}.

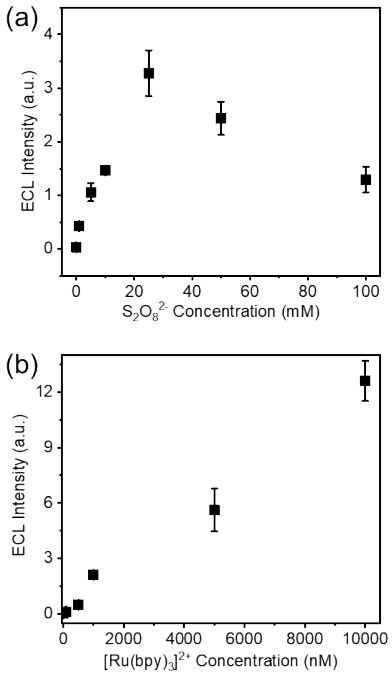

Figure 3. (a) Dependence of ECL intensity on peroxydisulfate concentration, 1 µM $[Ru(bpy)_3]^{2+}$ in PBS pH 7.4, integrated area of ECL from 10 s chronoamperometric (CA) pulse to -2.25 V. (b) Dependence of ECL intensity on $[Ru(bpy)_3]^{2+}$ concentration, 25 mM $S_2O_8^{2-}$, PBS pH 7.4, 5 s integrated area of ECL from 5 s CA pulse to -2.25 V. Error bars represent the standard deviation of three replicate determinations.

co-reactant in aqueous solutions and demonstrates the potential of $Ti_3C_2T_x$ MXene electrodes for use in analytical applications employing cathodic ECL (Figure 3b).

In conclusion, this work enhances the analytical sensitivity and versatility of the $[Ru(bpy)_3]^{2+}$-peroxydisulfate ECL system by exploiting the high conductivity and cathodic ECL of $Ti_3C_2T_x$ MXenes. The fabricated $Ti_3C_2T_x$ MXene electrodes demonstrate superior cathodic ECL intensity when compared to both BDD[8] and graphitic carbon SPEs and provide an alternative electrode material for the development of highly sensitive analytical detection strategies employing reductive-oxidation co-reactant ECL systems. This work lays the foundation for future analytical applications of $Ti_3C_2T_x$ MXene electrodes using cathodic ECL.

Acknowledgements

The authors acknowledge support from the Australian Research Council (FT130100380; DP200102947; DP18010094; IH140100018), the Australian National Fabrication Facility and the National Health and Medical Research Council of Australia (GNT1161573). This work was funded in part by the Office of Naval Research Global (N62909–18–1-2024).

Conflicts of interest

There are no conflicts to declare.

Notes and References

1. A. J. Bard, *Electrogenerated chemiluminescence*, CRC Press, 2004.
2. G. Valenti, A. Fiorani, H. Li, N. Sojic and F. Paolucci, *ChemElectroChem*, 2016, **3**, 1990-1997.
3. D. M. Hercules, *Science*, 1964, **145**, 808-809.
4. N. E. Tokel and A. J. Bard, *J. Am. Chem. Soc.*, 1972, **94**, 2862-2863.
5. W. Miao, J.-P. Choi and A. J. Bard, *J. Am. Chem. Soc.*, 2002, **124**, 14478-14485.
6. Y. Chen, S. Zhou, L. Li and J.-j. Zhu, *Nano Today*, 2017, **12**, 98-115.
7. H. B. Martin, A. Argoitia, U. Landau, A. B. Anderson and J. C. Angus, *J. Electrochem. Soc*, 1996, **143**, L133-L136.
8. A. Fiorani, Irkham, G. Valenti, F. Paolucci and Y. Einaga, *Anal. Chem.*, 2018, **90**, 12959-12963.
9. A. Sinha, Dhanjai, H. Zhao, Y. Huang, X. Lu, J. Chen and R. Jain, *TrAC, Trends Anal. Chem.*, 2018, **105**, 424-435.
10. L. Lorencová, T. Bertok, E. Dosekova, A. Holazová, D. Paprckova, A. Vikartovská, V. Sasinková, J. Filip, P. Kasák and M. Jerigová, *Electrochim. Acta*, 2017, **235**, 471-479.
11. Y. Fang, X. Yang, T. Chen, G. Xu, M. Liu, J. Liu and Y. Xu, *Sens. Actuators, B*, 2018, **263**, 400-407.
12. P. K. Kalambate, N. S. Gadhari, X. Li, Z. Rao, S. T. Navale, Y. Shen, V. R. Patil and Y. Huang, *TrAC, Trends Anal. Chem.*, 2019, **120**, 115643.
13. H. Zhang, Z. Wang, Q. Zhang, F. Wang and Y. Liu, *Biosens. Bioelectron.*, 2019, **124-125**, 184-190.
14. C. Zhang, B. Anasori, A. Seral-Ascaso, S.-H. Park, N. McEvoy, A. Shmeliov, G. S. Duesberg, J. N. Coleman, Y. Gogotsi and V. Nicolosi, *Adv. Mater.*, 2017, **29**, 1702678.
15. Z. Wang, S. Qin, S. Seyedin, J. Zhang, J. Wang, A. Levitt, N. Li, C. Haines, R. Ovalle-Robles, W. Lei, Y. Gogotsi, R. H. Baughman and J. M. Razal, *Small*, 2018, **14**, 1802225.
16. J. Zhang, S. Seyedin, S. Qin, Z. Wang, S. Moradi, F. Yang, P. A. Lynch, W. Yang, J. Liu, X. Wang and J. M. Razal, *Small*, 2019, **15**, 1804732.
17. J. Zhang, S. Uzun, S. Seyedin, P. A. Lynch, B. Akuzum, Z. Wang, S. Qin, M. Alhabeb, C. E. Shuck, W. Lei, E. C. Kumbur, W. Yang, X. Wang, G. Dion, J. M. Razal and Y. Gogotsi, *ACS Cent. Sci.*, 2020, **6**, 254-265.
18. M. Alhabeb, K. Maleski, B. Anasori, P. Lelyukh, L. Clark, S. Sin and Y. Gogotsi, *Chem. Mater.*, 2017, **29**, 7633-7644.
19. J. L. Hart, K. Hantanasirisakul, A. C. Lang, B. Anasori, D. Pinto, Y. Pivak, J. T. van Omme, S. J. May, Y. Gogotsi and M. L. Taheri, *Nat. Commun.*, 2019, **10**, 522.
20. T. Schultz, N. C. Frey, K. Hantanasirisakul, S. Park, S. J. May, V. B. Shenoy, Y. Gogotsi and N. Koch, *Chem. Mater.*, 2019, **31**, 6590-6597.
21. K. Maleski, C. E. Ren, M.-Q. Zhao, B. Anasori and Y. Gogotsi, *ACS Appl. Mater. Interfaces*, 2018, **10**, 24491-24498.
22. D. F. Baker and R. H. Bragg, *J. Non-Cryst. Solids*, 1983, **58**, 57-69.
23. A. J. Bard, L. R. Faulkner, J. Leddy and C. G. Zoski, *Electrochemical methods: fundamentals and applications*, wiley New York, 1980.
24. R. O. Kadara, N. Jenkinson and C. E. Banks, *Sensor. Actuat. B-Chem.*, 2009, **138**, 556-562.
25. R. O. Kadara, N. Jenkinson, B. Li, K. H. Church and C. E. Banks, *Electrochem. Commun.*, 2008, **10**, 1517-1519.
26. A. G. Theakstone, E. H. Doeven, X. A. Conlan, L. Dennany and P. S. Francis, *Chem. Commun.*, 2019, **55**, 7081-7084.
27. J.-P. Choi and A. J. Bard, *Anal. Chim. Acta*, 2005, **541**, 141-148.
28. A. Fiorani, G. Valenti, Irkham, F. Paolucci and Y. Einaga, *Phys. Chem. Chem. Phys.*, 2020, DOI: 10.1039/D0CP02005B.
29. P.-P. Dai, T. Yu, H.-W. Shi, J.-J. Xu and H.-Y. Chen, *Anal. Chem.*, 2015, **87**, 12372-12379.
30. Q. Zhai, J. Li and E. Wang, *ChemElectroChem*, 2017, **4**, 1639-1650.
31. Z. Wu, J. Hu, T. Zeng, Z.-L. Zhang, J. Chen, G. Wong, X. Qiu, W. Liu, G. F. Gao, Y. Bi and D.-W. Pang, *Anal. Chem.*, 2017, **89**, 2039-2048.
32. Y.-M. Lei, R.-X. Wen, J. Zhou, Y.-Q. Chai, R. Yuan and Y. Zhuo, *Anal. Chem.*, 2018, **90**, 6851-6858.
33. C. Tian, L. Wang, F. Luan, X. Fu, X. Zhuang and L. Chen, *Chem. Commun.*, 2019, **55**, 12479-12482.
34. X.-L. Huo, H. Yang, M.-X. Li, W. Zhao, J.-J. Xu, Y. Wang, X.-L. Luo and H.-Y. Chen, *Nanoscale*, 2018, **10**, 19224-19230.
35. Q. Lan, Q. Li, X. Zhang and Z. Chen, *J. Electroanal. Chem.*, 2018, **810**, 216-221.
36. Irkham, T. Watanabe, A. Fiorani, G. Valenti, F. Paolucci and Y. Einaga, *J. Am. Chem. Soc.*, 2016, **138**, 15636-15641.
37. G. Valenti, E. Rampazzo, S. Kesarkar, D. Genovese, A. Fiorani, A. Zanut, F. Palomba, M. Marcaccio, F. Paolucci and L. Prodi, *Coord. Chem. Rev.*, 2018, **367**, 65-81.
38. H. S. White and A. J. Bard, *J. Am. Chem. Soc.*, 1982, **104**, 6891-6895.
39. C. Liang, Z.-S. Wang and C. J. Bruell, *Chemosphere*, 2007, **66**, 106-113.
40. A. Lewandowska-Andralojc and D. E. Polyansky, *J. Phys. Chem. A*, 2013, **117**, 10311-10319.
41. O. V. Reshetnyak, E. P. Koval'chuk, P. Skurski, J. Rak and J. Błażejowski, *J. Lumin.*, 2003, **105**, 27-34.
42. D. Ege, W. G. Becker and A. J. Bard, *Anal. Chem.*, 1984, **56**, 2413-2417.